Regulation of Ferroptosis in Obesity: Muscle Type-Specific Effects of Dietary Restriction and Exercise

Fujue Ji[1, 2], Haesung Lee[1, 2], and Jong-Hee Kim[1, 2, #]

[1] Department of Physical Education, College of Performing Arts and Sport, Hanyang University, 222 Wangsimni-ro, Seongdong-gu, Seoul, Republic of Korea

[2] BK21 FOUR Human-Tech Convergence Program, Hanyang University, 222 Wangsimni-ro, Seongdong-gu, Seoul 04763, Republic of Korea

[#] Corresponding Author

carachel07@hanyang.ac.kr

Background:

Obesity is a significant global health issue and a risk factor for numerous diseases. Ferroptosis, an iron-dependent regulated cell death, is triggered by iron overload and the excessive accumulation of lipid peroxidation mediated by reactive oxygen species. Studies has identified a strong association between ferroptosis and obesity. Additionally, dietary restriction (DR) and DR combined with exercise (DR+Ex) are effective strategies for managing obesity and ferroptosis. However, the regulation of ferroptosis and its signaling pathways in skeletal muscle under conditions of obesity, DR, and DR+Ex remains poorly understood.

Methods:

Mice were divided into four groups: normal diet, high-fat diet, high-fat DR, and high-fat DR+Ex. All mice were fed ad libitum with either a normal or high-fat diet for the first 14 weeks, followed by the respective interventions for the subsequent 8 weeks. Mice muscle ferroptosis were examined by immunohistochemistry, Hematoxylin & Eosin, Masson's trichrome, Prussian blue staining, and Western-Immunoblot.

Results:

The high-fat diet resulted in increased inflammatory cell infiltration, fibrosis, and iron accumulation. Red and white muscle showed increased expression of 4-HNE, regulated by GPX4 and NCAO4, respectively. DR and DR+Ex reduced downstream 4-HNE expression by regulating GPX4 in red muscle.

Conclusion:

Due to metabolic differences, obesity-induced ferroptosis in skeletal muscle and the regulation by DR+Ex exhibiting fiber type-specificity. Specifically, red and white muscle respond to obesity-induced ferroptosis through different pathways; red muscle can inhibit obesity-induced ferroptosis through DR+Ex by GPX4. This deepens the understanding of mechanisms related to skeletal muscle cell death and provides scientific data support for the personalized treatment of related diseases.

Keywords: Obesity, Ferroptosis, Muscle type-specific, Dietary restriction, Exercise

1. Introduction

Obesity has emerged as a significant global health issue, affecting millions of individuals worldwide. Its detrimental effects on human health are well-documented, with numerous studies linking it to chronic diseases such as cardiovascular disorders, type 2 diabetes, and certain types of cancer (Blüher, 2019). Recent research has found that various chronic diseases caused by obesity are related to its induction of multiple cell death pathways, including ferroptosis (Stockwell et al., 2017).

Ferroptosis is an iron-dependent form of regulated cell death caused by iron overload and the excessive accumulation of lipid peroxidation products mediated by reactive oxygen species (ROS) (Dixon et al., 2012). This unique cell death mechanism has been implicated in the pathogenesis of various diseases across different organs and tissues, including neurodegenerative disorders, liver diseases, and kidney injury (Stockwell & Jiang, 2019). Studies have found that obesity can lead to tissue or organ dysfunction and damage by regulating ferroptosis. Specifically, obesity regulates cellular ferroptosis by modulating iron, lipid, and amino acid metabolism signaling pathways, thereby inducing and worsening tissue or organ dysfunction and damage (He et al., 2023).

Skeletal muscle is the largest metabolic organ in the human body, playing a crucial role in energy metabolism and fat oxidation, and is thus an indispensable part of overall metabolic health (Franco-Romero et al., 2024; Mizushima, 2007). Studies have found that obesity can lead to skeletal muscle dysfunction and even diseases, such as contractile dysfunction and sarcopenic obesity (Collins et al., 2018; Kalinkovich & Livshits, 2017). Furthermore, ferroptosis-related signaling has been identified in diseases such as sarcopenia, rhabdomyolysis, rhabdomyosarcoma, and fatigue due to excessive exercise (Ding et al., 2021; Guerrero-Hue et al., 2019; Huang et al., 2021). These skeletal muscle diseases severely impact patients' quality of life and physical function, ultimately increasing mortality rates. These studies indicate that skeletal muscle health is closely related not only to obesity but also to ferroptosis. However, it remains unclear whether ferroptosis is involved in the negative regulation of skeletal muscle health by obesity. Additionally, skeletal muscle is composed of different muscle types (white and red), which exhibit distinct metabolic characteristics, and their responses to ferroptosis under obesity-induced stress are also unclear. Addressing these scientific questions will help us further understand the negative effects of obesity on skeletal muscle and provide new therapeutic strategies for treating related diseases in the future.

Dietary restriction (DR) has been extensively studied for its potential health benefits, not only ameliorates obesity-induced skeletal muscle dysfunction (Suga et al., 2014) but also regulated the signaling pathway associated with ferrpotosis (Fang et al., 2021). Exercise (Ex) is widely recognized for its positive impact on health (Ruegsegger & Booth, 2018), not only improves obesity-induced skeletal muscle dysfunction (Ostler et al., 2014) but also modulates the expression of ferroptosis signaling in the brain, kidney, and nerves (Chen et al., 2023; Liu et al., 2022; Xiang et al., 2023). Both CR and Ex demonstrate dual regulatory effects on obesity and ferroptosis. Moreover, dietary restriction combined with exercise (DR+Ex) is acknowledged as a method that

more effectively counteracts the negative effects of obesity and lipid peroxidation than DR or Ex alone (Khachatoorian & Samara, 2018; Kim et al., 1996; Kvedaras et al., 2020; Li et al., 2017). However, the regulatory effects of DR and DR+Ex on obesity-induced ferroptosis in skeletal muscle remain unclear. Addressing this gap can provide scientific data to support the development physical therapy for obesity- and ferroptosis-related skeletal muscle diseases in the future.

Therefore, this study will first reveal the regulatory mechanisms of obesity on ferroptosis in skeletal muscle. Subsequently, it will investigate the regulatory mechanisms of CR and CR+Ex on skeletal muscle ferroptosis induced by obesity. Understanding the molecular mechanisms underlying these processes could provide valuable insights into the development of targeted interventions for obesity-related muscle disorders and promote overall health and well-being.

2. Methods

2.1 Animals and Experimental Design

Male C57BL/6N mice (14-month-old) were randomly divided into four experimental groups: Normal diet (ND, n=7), High-fat diet (HF, n=7), 20% high-fat dietary restriction (HFR, n=7), and 20% high-fat dietary restriction with voluntary wheel running exercise (HFRV, n=7). For the first 4 months, all mice were fed either a standard chow diet (ND; Teklad Global 2018, Envigo Inc.) or a high-fat diet (HF; 45% kcal from fat, D12451, Research Diets Inc.) (Table 1). In the subsequent 4 months, dietary restriction (DR) and dietary restriction combined with exercise (DR+Ex) interventions were applied to the respective groups (Figure 1). The mice were housed in a controlled environment, maintained at a temperature of 22 ± 2 °C with 50–60% humidity, and subjected to a 12-hour light/dark cycle. All animals had ad libitum access to water and were allowed physical activity. The experimental procedures were approved by the Institutional Animal Care and Use Committee (IACUC) of Hanyang University (HYU 2021-0239A).

Table 1. Diet composition

Group	*ND*		*HF, HFR, and HFRV*	
Diet	*Teklad Global 2018, Envigo Inc.*		*D12451, Research Diets Inc.*	
	gm%	*kcal%*	*gm%*	*kcal%*
Protein	*18.4*	*30*	*24*	*20*
Carbohydrate	*44.2*	*50*	*41*	*35*
Fat	*6*	*20*	*24*	*45*
Total		*100*		*100*
Kacl/gm	*3.1*		*4.73*	

Figure 1. Schematic overview experimental study design.

2.2 Body Composition

Mice were anesthetized with 40 mg/kg ketamine and 0.8 mg/kg medetomidine and analyzed for body composition using an InAlyzer Dual-energy X-ray Absorptiometry (DEXA) system (Micro Photonics Inc., PA, USA). The parameters measured included total mass (g), lean mass ratio (%), fat mass (g), lean mass (g), fat content in tissue (%), and fat mass ratio (%).

2.3 Skeletal Muscle Function Tests

All mice underwent skeletal muscle function tests before euthanasia. Skeletal muscle function was assessed in four groups of mice using tests for walking speed, endurance, physical activity, and grip strength (Ji et al., 2024).

Rota-Rod test: Walking speed was assessed using the Rota-Rod test. An adaptation period was conducted during the first three days, involving a pre-test exercise at 5 rpm for 1 minute, once per day. The official test utilized an acceleration mode, where the speed increased from 5 to 50 rpm over a 5-minute period (Model 76-0770, Harvard Apparatus Inc., Holliston, MA, USA). The latency to fall from the device was recorded. Each mouse was tested three times with a ten-minute interval between tests, and the best performance out of the three trials was used as the outcome measure.

Treadmill test: Endurance capacity was evaluated using a treadmill test. Adaptation was performed three days before the official test, consisting of running at 5 cm/s for 5 minutes, once per day, on a 0-degree slope. During the official test, the treadmill speed increased by 1 cm/s every 20 seconds starting from 5 cm/s, with a 0-degree slope. The trial ended when the mouse touched the shock pad (set at 0.6 mA) three times.

Voluntary wheel test: Physical activity was measured using the voluntary wheel test. Running distance was recorded using a voluntary wheel (MAN86130, Lafayette Instrument Company, Lafayette, IN, USA), with each wheel rotation corresponding to a distance of 0.4 m. The average running distance over a 5-day period was recorded for each mouse.

Inverted-cling grip test: Grip strength was assessed using the inverted-cling grip test. Adaptation was conducted prior to the official test, with the adaptive test performed once a day for three days. During the official test, mice were placed in the center of a wire mesh screen, and a stopwatch was

started. The screen was then rotated to an inverted position over 2 seconds, with the mouse's head descending first, and held 40-50 cm above a padded surface. The time until the mouse fell was recorded. This measurement was repeated three times with ten-minute intervals between tests, and the maximum reading was recorded.

2.4 Preservation and Preparation of Skeletal Muscle

The anesthetized mice were euthanized by cervical dislocation. Following euthanasia, the gastrocnemius (GAS) muscle were carefully dissected from the mice. The left GAS was fixed in 10% formalin for 24 hours, then dehydrated and embedded in paraffin. Sections were prepared for Hematoxylin and Eosin (H&E) staining, Prussian blue staining, Masson's trichrome staining, and immunohistochemistry (IHC). The right GAS was snap-frozen in liquid nitrogen and stored at –80°C for subsequent Western-immunoblot (WB) analyses.

2.5 Hematoxylin and Eosin (H&E) staining

Rehydrated tissue sections (5 μm) were stained using ClearView™ hematoxylin (MA0101010, StatLab, McKinney, TX, USA) and ClearView™ eosin (MA0101015, StatLab, McKinney, TX, USA). Subsequently, the sections were dehydrated, cleared, and mounted with neutral resin. Images were acquired using a slide scanner (Axio Scan. Z1, Zeiss) at 200x magnification. For each mouse, a single section of GAS was randomly photographed to obtain 5 images, each covering an area of 0.271mm^2. The average of these five images was used to represent the cross-sectional area (CSA) of that GAS for the mouse. The CSA was automatically analyzed using "Cellpose," an open-source deep learning-based segmentation tool (Stringer et al., 2021).

2.6 Prussian Blue Staining

Rehydrated tissue sections (5 μm) were stained using Prussian Blue staining kit (G1422, Beijing Solarbio Science & Technology Co., Ltd.). Images were acquired using a slide scanner (Axio Scan. Z1, Zeiss) at 200x magnification. For each mouse, a single section of GAS was randomly photographed to obtain 5 images, each covering an area of 0.271mm^2. The average of these five images was used to represent the value of that iron accumulation for the mouse. ImageJ software was used for the analysis.

2.7 Masson's Trichrome Staining

Rehydrated tissue sections (5 μm) were stained using Masson's trichrome staining kit (G1340, Beijing Solarbio Science & Technology Co., Ltd.). Images were acquired using a slide scanner (Axio Scan. Z1, Zeiss) at 200x magnification. For each mouse, a single section of each GAS was randomly photographed to obtain 5 images, each covering an area of 0.271mm^2. The average of these five images was used to represent the ECM value of that GAS for the mouse. ImageJ software was used for analysis.

2.8 Western-Immunoblot (WB)

The red and white GAS were dissected separately (Chen et al., 2015). As previously described (Ji et al., 2024), the GAS was lysed using an EzRIPA Lysis Kit (WSE-7420, ATTO). Protein concentration was determined using the Pierce™ Bicinchoninic Acid Protein Assay Kit (Thermo Scientific, Waltham, MA, USA). Equal amounts of protein samples (40 μg) were separated by

168 sodium dodecyl sulfate-polyacrylamide gel electrophoresis and electro-transferred to
169 nitrocellulose membranes (Bio-Rad Laboratories, Hercules, CA, USA). The membranes were
170 blocked with 5% non-fat milk dissolved in Tris-buffered saline with Tween-20 (TBST; 10 mM
171 Tris, 150 mM NaCl, and 0.1% Tween-20; pH 7.6) for 1.5 hours at room temperature and then
172 incubated with primary antibodies (Table 2) overnight at 4°C. Subsequently, the membranes were
173 incubated with horseradish peroxidase-conjugated secondary antibodies (Table 2) for 1.5 hours at
174 room temperature. The targeted bands were quantified by densitometry using ImageJ software.

175 ***2.9 Immunohistochemistry (IHC)***

176 Following the immunohistochemistry protocol with modifications based on Magaki et al.,
177 paraffin-embedded tissue sections (5 μm) were deparaffinized and rehydrated (Magaki et al.,
178 2019). Heat-induced antigen retrieval was performed using 0.01 mol/L sodium citrate buffer (pH
179 6.0, C1010, Beijing Solarbio Science & Technology Co., Ltd.) in a microwave oven for 20
180 minutes at 100°C. The sections were then washed twice with Phosphate-buffered saline (PBS;
181 0.137M NaCl, 0.0027M KCL, 0.010mM Na_2HPO_4, and 0.002mM KH_2PO_4; pH 7.2) for 5 minutes
182 each and blocked with 3% hydrogen peroxide (4104-4400, DAE JUNG) for 15 minutes twice to
183 remove endogenous peroxidases. Following three additional 5-minute washes with PBS, the
184 sections were blocked with 100-200 μl of blocking buffer (5% Bovine serum albumin in PBS) for
185 30 minutes at room temperature. After blocking, the sections were washed three times with PBS
186 for 5 minutes each and incubated with the primary antibody (Table 2) overnight at 4°C. The
187 sections were then washed three times with PBS for 5 minutes each and incubated with the
188 secondary antibody (Table 2) in a humidified chamber for 60 minutes at room temperature.
189 Following three more 5-minute washes with PBS, the sections were incubated with the Pierce™
190 DAB Substrate Kit (Thermo Scientific, #34002) for 6 minutes and washed three times with PBS
191 for 5 minutes each. Finally, the sections were rehydrated and mounted. Images were acquired
192 using a slide scanner (Axio Scan. Z1, Zeiss) at 200x magnification. For each mouse, a single
193 section of each GAS was randomly photographed to obtain 5 images, each covering an area of
194 0.271mm^2. The average of these five images was used to represent the antibody expression value
195 of that GAS for the mouse. ImageJ software was used for analysis.

196 *Table 2. Primary and secondary antibodies.*

Antibodies	Source	Vender	Catalog	Dilution (WB)	Dilution (IHC)
P53	Rabbit	Cell signaling	30313	1:500	
SLC7A11	Rabbit	Abcam	ab175186	1:1000	
GAPDH	Rabbit	Cell signaling	5174	1:4000	
GPX4	Rabbit	Abcam	ab125066	1:1000	
AMPK	Rabbit	Cell signaling	5831	1:500	
TFR1	Rabbit	Abcam	ab84036	1:500	
NCOA4	Rabbit	Invitrogen	PA5-115626	1:500	
Rab7	Rabbit	Abcam	EPR7589	1:1000	
4-HNE	Rabbit	Abcam	ab46545	1:1000	1:200
MDA	Mouse	Abcam	ab243066	1:500	1:50
Goat anti Rabbit	Goat	Invitrogen	G-21234	1:5000	1:500
m-IgG Fc	-	SANTA	sc-525409	1:5000	1:25

2.10 Statistical Analysis

Statistical analyses were performed using GraphPad Prism software (version 9). Comparisons between two groups were conducted using an unpaired Student's t-test. For comparisons among three groups, a one-way analysis of variance (ANOVA) followed by a least significant difference (LSD) post-hoc test was employed. To assess the effects of muscle type (white vs. red) and dietary conditions (HF vs. DR vs. DR+Ex), a two-way ANOVA with Bonferroni's post-hoc test was applied. Outliers were identified and removed using the Z-score approach prior to conducting statistical analyses to ensure the robustness and reliability of the results. All results are expressed as the mean ± standard deviation (SD). Statistical significance was set at $p < 0.05$, with asterisks indicating the following levels of significance: *$p < 0.05$, **$p < 0.01$, ***$p < 0.001$, and ****$p < 0.0001$.

3. Results

3.1 Obesity Evokes Dysfunction and Ferroptosis in Skeletal Muscle

To investigate whether obesity regulates ferroptosis in skeletal muscle, we induced obesity in mice by feeding them a high-fat diet for 14 weeks. All the data are shown in Figure 2.

DEXA analysis revealed that high-fat diet intake led to increases in body weight ($P < 0.0001$), lean mass ($P = 0.0021$), fat mass ($P < 0.0001$), fat mass ratio ($P < 0.0001$), and fat mass in tissues ($P < 0.0001$), while the lean mass ratio decreased ($P < 0.0001$) (Figure 2A-H). These indicators are widely used to evaluate and identify mouse models of obesity (Chen et al., 2012; Koza et al., 2006; Y. Yang et al., 2014; Yeu et al., 2019). Consistent with impaired skeletal muscle function in obese mice (Graham et al., 2019; Vellers et al., 2017), we found that a high-fat diet significantly reduced walking speed ($P = 0.0424$), grip strength ($P = 0.0053$), and endurance in mice ($P = 0.0217$) (Figure 2I-K). These findings further validate the successful establishment of the obese mouse model.

Histological features of ferroptosis include the accumulation of inflammatory cells in tissues (Zhang et al., 2023) and fibrosis (Yu et al., 2020). H&E staining revealed that although the CSA of HF skeletal muscle significantly increased ($P = 0.00210$), it was accompanied by substantial inflammatory cell infiltration (Figure 2M and R). Additionally, Masson's trichrome staining indicated a significant increase in skeletal muscle fibrosis in HF compared to NDC ($P = 0.0110$) (Figure 2N and R). Ferroptosis is highly associated with lipid peroxidation and abnormal iron accumulation (Dixon et al., 2012). As markers of lipid peroxidation, malondialdehyde (MDA) and 4-hydroxynonenal (4-HNE) can reflect the extent of ferroptosis in cells (Chen et al., 2021; Tang et al., 2021). IHC analysis showed elevated levels of lipid peroxidation products 4-HNE ($P = 0.0320$) and MDA ($P = 0.0150$) in HF skeletal muscle compared to NDC (Figure 2Q-P and R). Furthermore, Prussian blue staining revealed abnormal iron accumulation in HF skeletal muscle ($P = 0.0210$) (Figure 2Q and R). These data indicate that obesity, leading to skeletal muscle dysfunction and ferroptosis.

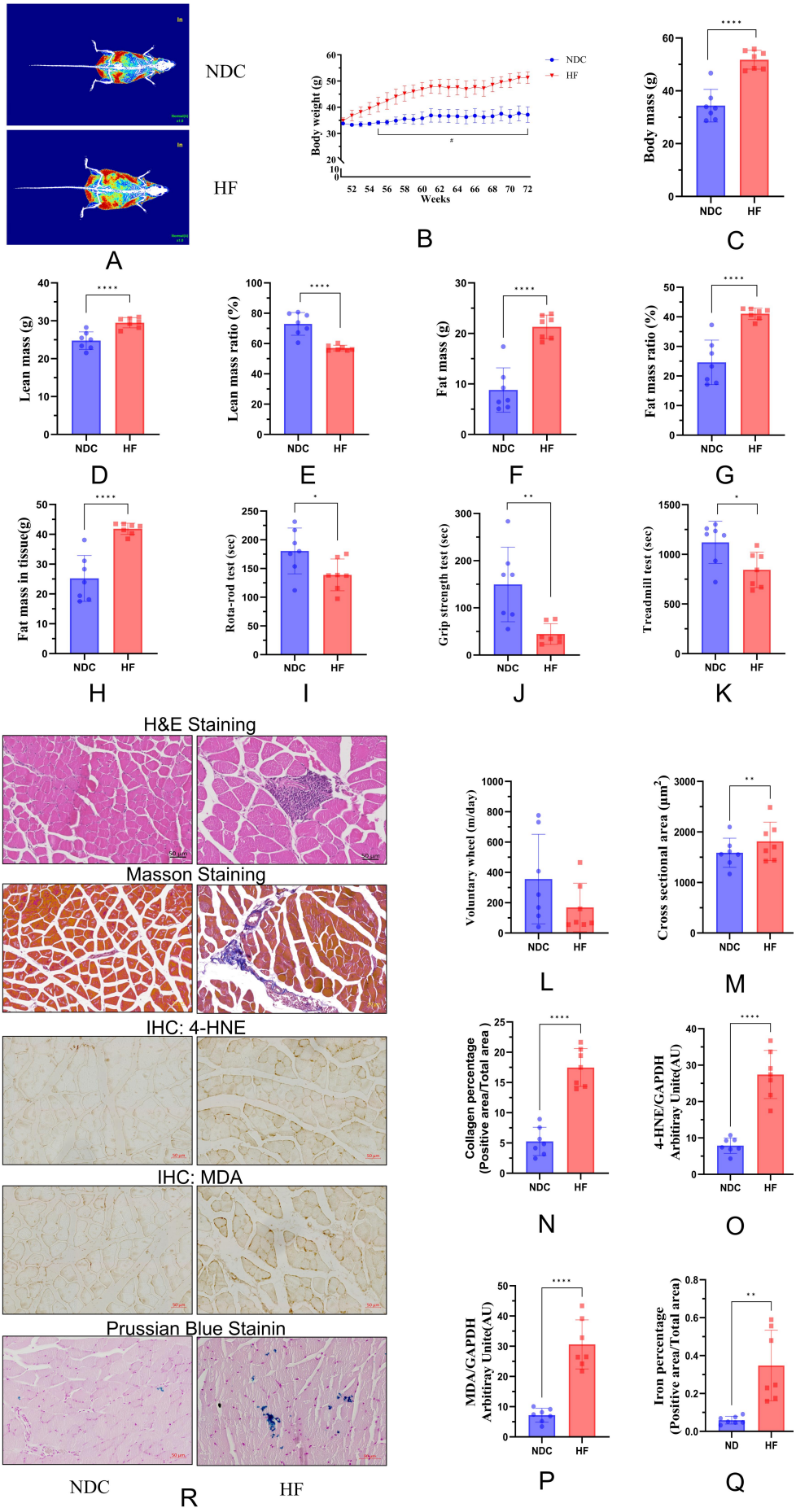
NDC
HF
A
Body weight (g)
Weeks
NDC
HF
B
Body mass (g)
C
Lean mass (g)
D
Lean mass ratio (%)
E
Fat mass (g)
F
Fat mass ratio (%)
G
Fat mass in tissue(g)
H
Rota-rod test (sec)
I
Grip strength test (sec)
J
Treadmill test (sec)
K
H&E Staining
Masson Staining
IHC: 4-HNE
IHC: MDA
Prussian Blue Stainin
NDC
R
HF
Voluntary wheel (m/day)
L
Cross sectional area (μm²)
M
Collagen percentage (Positive area/Total area)
N
4-HNE/GAPDH Arbitiray Unite(AU)
O
MDA/GAPDH Arbitiray Unite(AU)
P
Iron percentage (Positive area/Total area)
Q

Figure 2. High-fat diet-induced obesity evokes dysfunction and ferroptosis in skeletal muscle. (A) Representative DEXA-scanned images of NDC and HF mice; skeletal muscle, fat tissue, and bone are shown in blue, red, and white, respectively. (B) Weekly body weight changes (group × weeks): NDC vs. HF (, 54-72 weeks). (C-H) Quantitative data of final total mass, lean mass, lean mass ratio, fat mass, fat mass ratio, and fat mass in tissue, respectively, were acquired by DEXA scanning. (I-L) Skeletal muscle function tests. (I) Walking speed test. (J) Strength test. (K) Endurance test. (L) Physical activity test. (M) Skeletal muscle cross-sectional area in NDC and HF. (N) Skeletal muscle collagen area in NDC and HF. (O) 4-HNE expression levels in skeletal muscle. (P) MDA expression levels in skeletal muscle. (Q) Iron percentage in skeletal muscle. (R) Representative images showing H&E staining, Masson's trichrome staining, IHC, and Prussian blue staining of GAS. Significant differences are denoted by asterisks: $p < 0.05$ (*), $p < 0.01$ (**), $p < 0.001$ (***), and $p < 0.0001$ (****). All values are presented as mean ± SD. Normal diet control (NDC, n=7, 20.5-month-old), high-fat diet (HF, n=7, 20.5-month-old). Scale bar = 50 μm.*

3.2 Muscle Type-Specific Regulation of Ferroptosis by GPX4 and NCOA4 in Obesity

Given the observed ferroptosis in skeletal muscle as a result of obesity, we employed WB analysis to investigate the impact of obesity on the expression of representative proteins in 3 ferroptosis-related signaling pathways: amino acid, lipid, and iron metabolism in different muscle types. All the data are shown in Figure 3.

Under normal diet, the expression of glutathione peroxidase 4 (GPX4) ($P = 0.0073$) and nuclear receptor coactivator 4 (NCOA4) ($P = 0.0007$) was significantly higher and 4-HNE ($P = 0.002$) was lower in white compared to red muscle (Figure 3A and H). Under high-fat diet, the expression of NCOA4 was significantly lower in white compared to red muscle ($P < 0.0001$) (Figure 3G). Additionally, within the same muscle type, a high-fat diet significantly decreased the expression of GPX4 ($P = 0.0007$) and NCOA4 ($P = 0.0015$), and increased 4-HNE ($P < 0.0001$) in white muscle compared to a normal diet ($P < 0.05$) (Figure 3A, G, and H). Although a high-fat diet did not alter the expression of GPX4 in red muscle, it significantly increased the expression of NCOA4 ($P < 0.0001$) and 4-HNE ($P = 0.0375$) (Figure 3A, G, and H). These data indicated that the regulation of ferroptosis by obesity exhibits skeletal muscle type-specificity. Specifically, obesity regulates ferroptosis by decreasing the GPX4 expression in white muscle and increasing the NCOA4 in red.

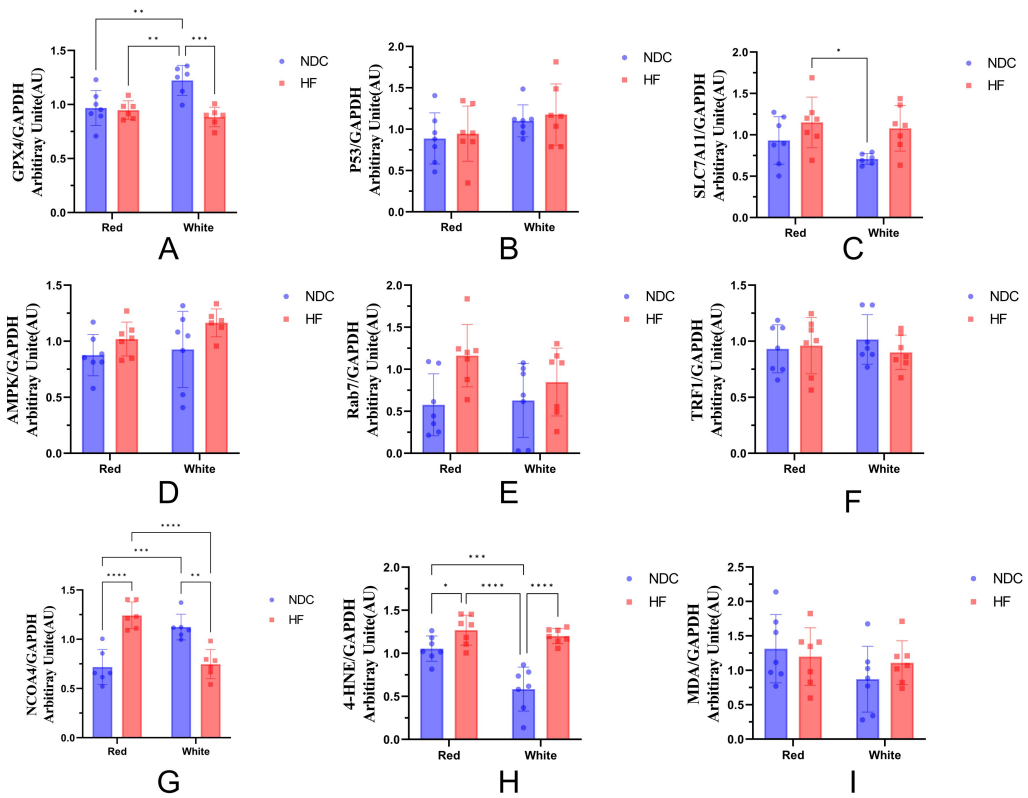

Figure 4. Muscle type-specific regulation of ferroptosis by GPX4 and NOCA4 in high-fat diet-induced obese mice. WB was performed for protein expression levels of ferroptosis signaling pathways, (A): Glutathione peroxidase 4 (GPX4), (B): P53, (C): Solute Carrier Family 7 Member 11 (SLC7A11), (D): AMP-activated protein kinase (AMPK), (E): Ras-related protein Rab-7a (Rab7), (F): Telomeric repeat-binding factor 1 (TRF1), (G) Nuclear Receptor Coactivator 4 (NCOA4), (H): 4-Hydroxynonenal (4-HNE), and (I): Malonaldehyde (MDA). Significant differences are denoted by asterisks: $p < 0.05$ (*), $p < 0.01$ (**), $p < 0.001$ (***) and $p < 0.0001$ (****). All values are presented as mean ± SD. Normal diet control (NDC, n=7, 20.5-month-old), high-fat diet (HF, n=7, 20.5-month-old).

3.3 DR and DR+Ex Show Improvement and Regulation in Physical Phenotypes and Ferroptosis in Obesity

We identified the regulatory effect of obesity on ferroptosis in skeletal muscle, and subsequently will investigate the intervention mechanisms of DR and DR+Ex on this process. This is because previous studies have widely reported the positive effects of DR and DR+Ex on obesity, lipid peroxidation, and even ferroptosis (Bevilacqua et al., 2005; Chen et al., 2023; Li et al., 2017; Liu et al., 2022; Walsh et al., 2014). All the data are shown in Figure 4.

Results showed significant differences in body weight between the HF and HFRV groups at 70 weeks (P = 0.0435) (Figure 4B). Compared to the HF, the HFRV significantly reduced total mass (P = 0.0061), lean mass (P = 0.0171), and fat mass in mice (P = 0.0159), but there were no changes in lean mass ratio, fat mass ratio, or fat mass in tissues (Figure 4C-H). DR and DR+Ex did not appear to effectively improve skeletal muscle function in the HF, HFR, and HFRV groups (Figure 4I-L).

Additionally, H&E staining showed that DR and DR+Ex reduced inflammatory cell infiltration in muscle fibers; however, DR+Ex also decreased the CSA of skeletal muscle ($P = 0.0296$) (Figure 4M and R). Masson's trichrome staining and Prussian blue staining indicated fibrosis and iron in skeletal muscle were not significant changes (Figure 4N, Q, and R). Lastly, IHC analysis showed no significant differences in the expression of 4-HNE and MDA among the HF, HFR, and HFRV groups (Figure 4O, P, and R). These data suggest that intervention of DR and DR+Ex has limited effects on improving and regulating physical phenotypes and ferroptosis in obese.

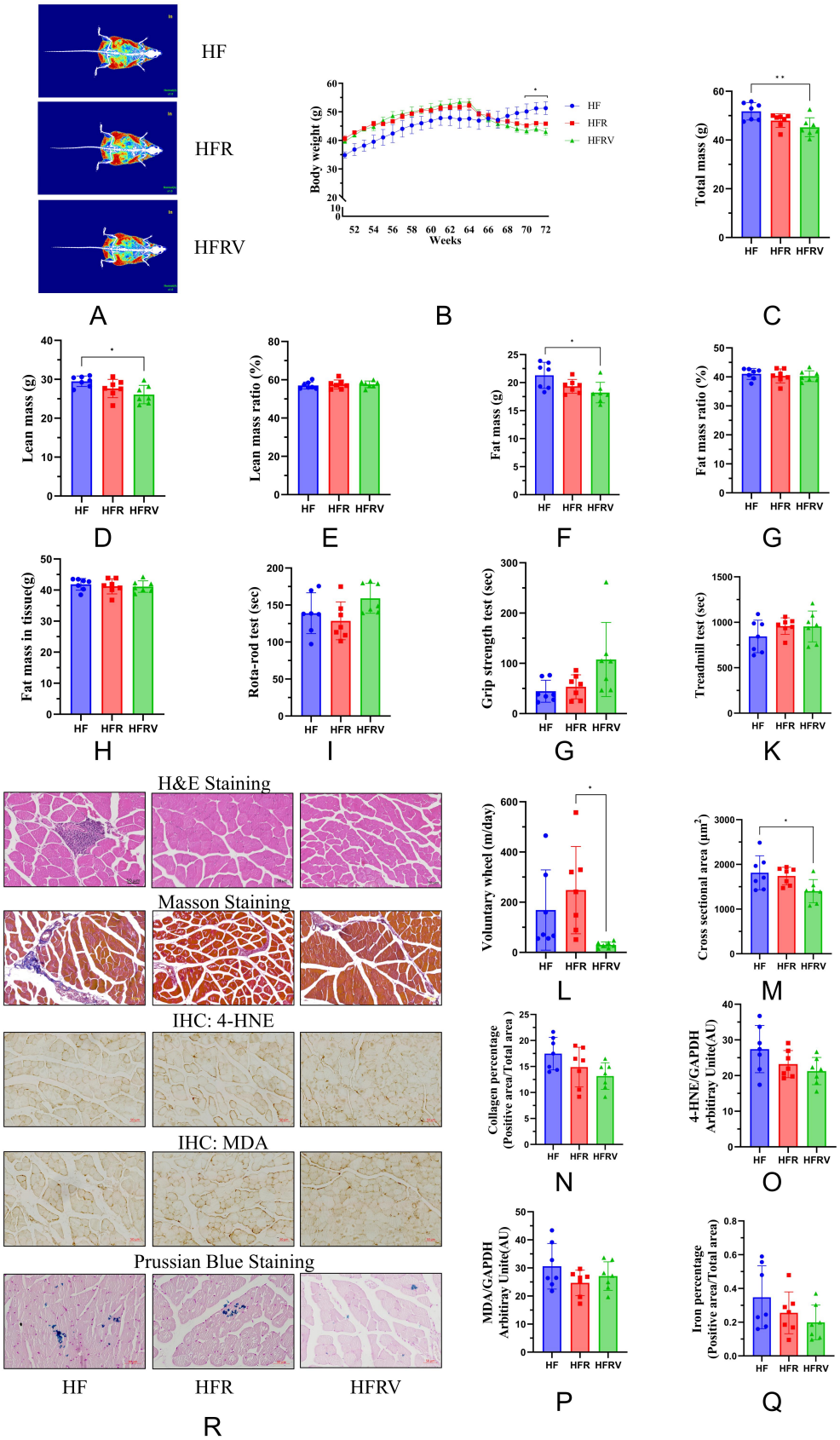

Figure 4. DR and DR+Ex Show Improvement and Regulation in Physical Phenotypes and Ferroptosis in Obesity. A) Representative DEXA-scanned images of NDC and HF mice; skeletal muscle, fat tissue, and bone are shown in blue, red, and white, respectively. (B) Weekly body weight changes (group × weeks): NDC vs. HF (, 54-72 weeks).*

(C-H) Quantitative data of final total mass, lean mass, lean mass ratio, fat mass, fat mass ratio, and fat mass in tissue, respectively, were acquired by DEXA scanning. (I-L) Skeletal muscle function tests. (I) Walking speed test. (J) Strength test. (K) Endurance test. (L) Physical activity test. (M) Skeletal muscle cross-sectional area in NDC and HF. (N) Skeletal muscle collagen area in NDC and HF. (O) 4-HNE expression levels in skeletal muscle. (P) MDA expression levels in skeletal muscle. (Q) Iron percentage in skeletal muscle. (R) Representative images showing H&E staining, Masson's trichrome staining, IHC, and Prussian blue staining of GAS. Significant differences are denoted by asterisks: $p < 0.05$ (*), $p < 0.01$ (**), $p < 0.001$ (***), and $p < 0.0001$ (****). All values are presented as mean ± SD. High-fat diet (HF, n=7, 20.5-month-old), 20% high-fat dietary restriction (HFR, n=7, 20.5-month-old), 20% high-fat dietary restriction with voluntary wheel running exercise (HFRV, n=7, 20.5-month-old). Scale bar = 50 μm.

3.4 Muscle Type-Specific Regulation of Ferroptosis by GPX4 Through DR and DR+Ex in High-Fat Diet-Induced Obese Mice

Although no significant differences were observed in the histological markers related to ferroptosis, a reduction was noted. Moreover, the detailed of CR and CR+Ex regulatory effects on muscle type-specific ferroptosis are not well understood. Therefore, it is worthwhile to further explore the muscle type-specific regulation of ferroptosis by these interventions through different pathways. The results of the WB analysis are shown in Figure 5.

Under the CR+Ex, the expression of 4-HNE in white muscle was significantly higher compared to red muscle ($P < 0.0001$) (Figure 5H). In red muscle, the expression of GPX4 was significantly higher in the HFRV group compared to the HF group ($P = 0.0471$) (Figure 5A); the expression of 4-HNE decreased sequentially in the HF, HFR, and HFRV groups, with significant differences ($P < 0.0001$ and $P = 0.0136$) (Figure 5H). In white muscle, the expression of AMP-activated protein kinase (AMPK) was significantly lower in the HFRV group compared to the HF ($P = 0.0086$) and HFR ($P = 0.0126$) groups (Figure 5D), and there were significant differences in the expression of 4-HNE between the HFR and HFRV groups ($P = 0.0427$) (Figure 5H). These data suggest that the regulation of ferroptosis by intervention in high-fat diet-induced obese mice is muscle type-specificity. Specifically, DR+Ex inhibits obesity-induced skeletal muscle ferroptosis by increasing the expression of GPX4 in red muscle.

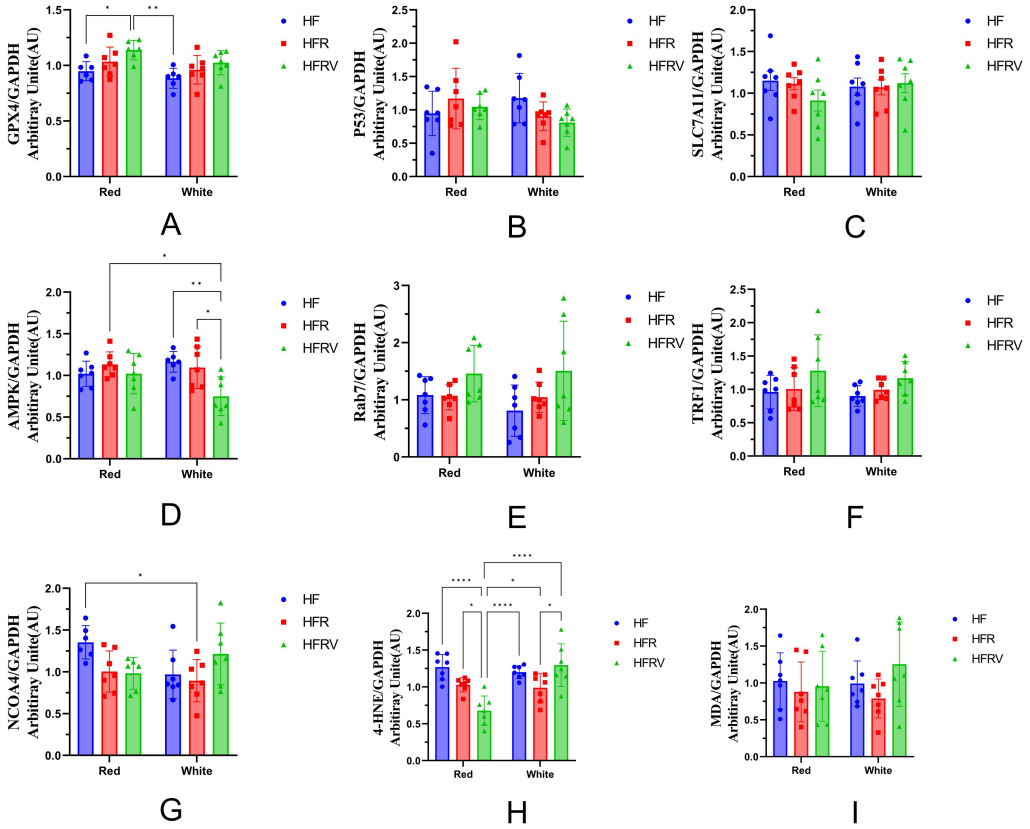

Figure 6. Through CR and CR+Ex muscle type-specific regulation of ferroptosis by GPX4 in high-fat diet-induced obese mice. WB was performed for protein expression levels of ferroptosis signaling pathways, (A): Glutathione peroxidase 4 (GPX4), (B): P53, (C): Solute Carrier Family 7 Member 11 (SLC7A11), (D): AMP-activated protein kinase (AMPK), (E): Ras-related protein Rab-7a (Rab7), (F): Telomeric repeat-binding factor 1 (TRF1), (G) Nuclear Receptor Coactivator 4 (NCOA4), (H): 4-Hydroxynonenal (4-HNE), and (I): Malonaldehyde (MDA). Significant differences are denoted by asterisks: $p < 0.05$ (*), $p < 0.01$ (**), $p < 0.001$ (***) and $p < 0.0001$ (****). All values are presented as mean ± SD. High-fat diet (HF, n=7), 20% high-fat diet dietary restriction (HFR, n=7), and 20% high-fat diet dietary restriction + voluntary wheel running exercise (HFRV, n=7).

4. Discussion

In recent years, the issue of dysfunction in cells, tissues, and organs caused by obesity has garnered widespread attention. Obesity-induced ferroptosis is considered one of the primary causes of these dysfunctions (Ganz, 2012; Ma et al., 2017; Orr et al., 2014; Zhao et al., 2022). Understanding the regulatory mechanisms of ferroptosis in obesity is significant clinical importance for skeletal muscle-related dysfunction and diseases. This study investigated the impact of obesity on ferroptosis in specific muscle types and the response mechanisms of its signaling pathways to DR and DR+Ex. Our research found that obesity can induce ferroptosis in skeletal muscle, while DR and DR+Ex can regulate this process. More importantly, the regulation of ferroptosis by obesity and its response to intervention are muscle type-specificity. These findings enhance our understanding of the mechanisms of obesity and ferroptosis, providing a scientific basis for further in-depth studies of these diseases and cell death mechanisms.

4.1 Appropriateness of an Obesity Mouse Model

342 Mice at 14-month-old and 20.5-month-old are approximately equivalent to humans aged 30-40
343 and 60-70 years (Justice et al., 2016). Research has shown that the prevalence of obesity in
344 humans increases significantly after about 35 years of age, reaching a peak around 65 years
345 (Chooi et al., 2019). In our study, mice were fed a high-fat diet starting at 14-month-old and
346 continuing until 20.5-month-old, to simulate sustained obesity in humans beginning at age 35 and
347 persisting until age 65. This experimental design better aligns with the prevalence trends of human
348 obesity, yielding more accurate preclinical data to inform clinical research or the treatment of
349 obesity-induced skeletal muscle-related diseases.

350 We induced an obese mouse model through 4 months of a high-fat diet (D12451, Research Diets
351 Inc.). This diet has been widely used in the construction of obese mouse models (Armani et al.,
352 2014; Han et al., 2006; Yongbin Yang et al., 2014). Although there is no precise definition for
353 high-fat diet-induced obese mouse models, the vast majority of studies use at least 8 weeks of ad
354 libitum high-fat diet to create obese mouse models (Buettner et al., 2007; Han et al., 2006; Hariri
355 & Thibault, 2010). Additionally, after analyzing the body composition of the mice using DEXA,
356 we found significant increases in body weight, lean mass, fat mass, fat mass in tissues, and fat
357 mass ratio following the high-fat diet. These changes in body composition are consistent with the
358 characteristics of obese mice reported in previous studies (Lin et al., 1977; Mandarim-de-Lacerda
359 et al., 2021; Rogers & Webb, 1980). Moreover, obesity leads to a decline in certain skeletal muscle
360 functions, which is also in line with prior research, indicating that dysfunctional skeletal muscle is
361 a hallmark of obesity (Shortreed et al., 2009; Zhang et al., 2015). Therefore, we conclude that a
362 4-month high-fat diet can successfully induce obesity, providing an experimental animal model for
363 subsequent study.

364 ***4.2 Obesity Evokes Ferroptosis in Skeletal Muscle***

365 Recent studies suggest that inflammatory cell infiltration is a hallmark of ferroptosis. Ferroptosis
366 causes lipid peroxidation of cell membranes and cell rupture, and the release of cellular contents
367 (such as high-mobility group protein B1) can activate a local inflammatory response, leading to
368 inflammatory cell infiltration. The study by Dixon et al. pointed out the potential inflammatory
369 role of ferroptosis in various diseases (Dixon et al., 2012). These research findings strongly
370 support that ferroptosis is accompanied by inflammatory cell infiltration. For instance, research by
371 Friedmann Angeli et al. (Friedmann Angeli et al., 2014) demonstrated that ferroptosis leads to
372 acute renal failure, accompanied by significant inflammatory cell infiltration. In the liver, where
373 ferroptosis occurs, inflammatory cell infiltration is also present, as shown in the hemochromatosis
374 mouse model study by Wang et al. (Wang et al., 2017).

375 Recently, the relationship between ferroptosis and tissue organ fibrosis has been explored in
376 several studies. Ferroptosis, an iron-dependent form of cell death, releases oxidized lipids and
377 cellular contents that can activate fibroblast proliferation, thereby promoting fibrosis. Specifically,
378 cellular contents released during ferroptosis, such as high-mobility group protein B1, can activate
379 fibroblasts and bone marrow-derived fibroblast-like cells. These cells, once activated, secrete large
380 amounts of ECM components like collagen, leading to tissue fibrosis (Kang et al., 2016; Wenzel et
381 al., 2017). Moreover, ferroptosis can activate nuclear factor kappa B (NF-κB) and other
382 pro-inflammatory signaling pathways, promoting the release of pro-fibrotic factors (Dixon et al.,

2012; Stockwell et al., 2017). Therefore, ferroptosis is considered a key pathological mechanism in liver and heart fibrosis (Fang et al., 2020; Friedmann Angeli et al., 2014).

Prussian blue staining revealed a significant increase in iron accumulation in the skeletal muscle of obesity. Studies have shown that obese individuals often exhibit lower serum iron levels and elevated hepcidin levels (Ganz, 2012). This increase in hepcidin inhibits iron absorption and release, leading to iron accumulation in the body (Ganz, 2012). Additionally, pro-inflammatory factors secreted in obesity, not only stimulate hepcidin synthesis but also directly affect iron metabolism, increasing iron accumulation in cells and tissues (Hotamisligil, 2006; Weisberg et al., 2003). Ferroptosis is an iron-dependent form of cell death, and its extent can be reflected by the amount of iron accumulation in cells, tissues, and organs. Iron accumulation is a critical trigger for ferroptosis. Excess intracellular iron generates large amounts of ROS through the Fenton Reaction, which induce lipid peroxidation and thereby trigger ferroptosis (Dixon et al., 2012; Stockwell et al., 2017). These research findings strongly support that iron accumulation caused by obesity is one of the factors inducing ferroptosis.

Ferroptosis is accompanied by the accumulation of lipid peroxides and oxidative stress (Dixon et al., 2012). This process is closely related to the expression of 4-HNE and MDA, as both compounds are markers of lipid peroxidation (He et al., 2022; Park et al., 2021). 4-HNE is a highly reactive aldehyde compound produced by lipid peroxidation, primarily derived from the peroxidation of ω-6 polyunsaturated fatty acids (Ayala et al., 2014). It can form adducts with proteins, DNA, and phospholipids, altering their structure and function, thereby causing cellular damage (Murdolo et al., 2023). Similarly, MDA, another product of lipid peroxidation, is commonly used to measure oxidative stress levels. High levels of MDA indicate lipid damage to cell membranes and altered cellular function (Ahmed et al., 2016; Savira et al., 2020). Iron generates highly reactive hydroxyl radicals (•OH) through the Fenton Reaction, which further induce lipid peroxidation, increasing the production of 4-HNE and MDA, enhancing oxidative stress within cells, and promoting ferroptosis (Endale et al., 2023). Thus, the expression levels of 4-HNE and MDA can indirectly reflect ferroptosis activity in tissues and organs.

In summary, obesity leads to inflammation cell infiltration, fibrosis, iron accumulation, and increased lipid peroxides in skeletal muscle. The phenomenon occurrence of these phenomena can confirm that obesity induces ferroptosis in skeletal muscle (Stockwell, 2022).

4.3 Regulation of Muscle Type-Specific Ferroptosis Signaling Pathways by Obesity

To better explore the regulatory mechanisms of ferroptosis in skeletal muscle induced by obesity, we used WB to examine the expression of ferroptosis signaling pathways in different types of muscle.

GPX4 plays a key regulatory role in ferroptosis through amino acid metabolism by inhibiting the cell death process via the reduction of lipid peroxides accumulation (Stockwell et al., 2017). The deficiency or inactivation of GPX4 leads to an increase in lipid peroxides, thereby triggering ferroptosis (W. S. Yang et al., 2014). In obesity, the expression of GPX4 in white muscle significantly decreases, while its expression in red muscle remains unaffected. This may be due to

422 the higher sensitivity of white muscle to lipid peroxidation. A high-fat diet increases oxidative
423 stress in white muscle, leading to GPX4 depletion, whereas red muscle, with its stronger
424 antioxidant capacity, can maintain GPX4 levels (Katunga et al., 2015; Zhuang et al., 2021).
425 Additionally, higher metabolic activity and lipid accumulation in white muscle may also
426 contribute to the significant decrease in GPX4 expression (Shi et al., 2024).

427 NCOA4 mediates ferritinophagy, the process of degrading ferritin to release stored iron, thereby
428 increasing intracellular free iron content. This promotes iron-catalyzed Fenton Reactions, leading
429 to lipid peroxidation and ferroptosis (Dowdle et al., 2014; Mancias et al., 2014). Studies have
430 shown that the absence of NCOA4 significantly reduces the occurrence of ferroptosis, further
431 demonstrating its crucial role in the ferroptosis process (Dowdle et al., 2014; Mancias et al., 2014).
432 Obesity impacts the expression of NCOA4 differently in red and white muscles, with an increase
433 in red muscle and a significant decrease in white muscle. White muscle primarily relies on
434 anaerobic metabolism and is more sensitive to lipid peroxidation and metabolic stress. The
435 increased metabolic stress caused by a high-fat diet enhances the white muscle cells' need for
436 oxidative stress defense, possibly downregulating NCOA4 expression to reduce ferritinophagy
437 activities, thereby protecting the cells damage from further ferroptosis. This hypothesis requires
438 further in-depth research.

439 Obesity leads to increased lipid accumulation and oxidative stress in both red and white muscles,
440 significantly enhancing the production of 4-HNE (Hart et al., 2018; Shi et al., 2024). Obesity also
441 weakens antioxidant defense mechanisms, such as reducing the activity of glutathione and
442 superoxide dismutase, further exacerbating lipid peroxidation (Hart et al., 2018). It is of
443 paramount importance to note that the skeletal muscle type specific expression of GPX4 and
444 NCOA4 as upstream and regulatory signals of 4-HNE was significantly modulated by
445 high-fat-induced obesity. Consequently, we propose that the upregulation of 4-HNE in red and
446 white muscle due to high-fat induced obesity is caused by significant alterations in the expression
447 of NCOA4 and GPX4, separately.

448 In obesity, the expression of 4-HNE significantly increased in both red and white muscles,
449 whereas the expression of MDA did not show significant changes. This discrepancy may be due to
450 the differences in the generation and metabolism processes of 4-HNE and MDA. The production
451 of 4-HNE is highly influenced by ROS. Obesity increases lipid peroxidation reactions and ROS
452 production, thereby significantly elevating 4-HNE levels (Morris et al., 2008; Ramana et al., 2014).
453 Additionally, 4-HNE is highly reactive and can form stable adducts with various biomolecules
454 such as proteins, DNA, and phospholipids, leading to its accumulation in tissues (Ayala et al.,
455 2014; Morris et al., 2008). However, the production of MDA is relatively stable, and its metabolic
456 pathways are more diverse and efficient. For example, MDA can be metabolized through various
457 pathways, such as being converted into water-soluble products by glutathione-S-transferase for
458 excretion or being transformed into less reactive compounds (Esterbauer et al., 1991). These
459 metabolic pathways maybe result in insignificant changes in MDA levels under obesity (Del Rio
460 et al., 2005).

461 Additionally, experimental techniques can affect the expression of MDA. When using IHC and

WB to detect MDA, IHC showed a significant increase in MDA after a high-fat diet, whereas WB did not show the same results. This discrepancy may arise from differences in the sensitivity and specificity of the detection methods (Del Rio et al., 2005). IHC can detect local accumulation of MDA in specific cell types or tissue regions, while WB measures overall protein levels, which may dilute signals of local high expression. Furthermore, differences in sample processing and extraction methods may lead to dilution or degradation of locally high concentrations of MDA in WB, affecting the detection results. These factors collectively explain why IHC can show a significant increase in MDA after a high-fat diet, while WB does not detect the same changes.

4.4 Regulation of Ferroptosis by DR and DR+Ex

We found that after 8 weeks of intervention, although some physical phenotypes and ferroptosis-related characteristics of the mice improved, there was no significant difference. This may be related to the intensity of the intervention and the metabolism of mice. Higher-intensity caloric restriction can produce more pronounced positive effects, but it is not suitable for aged mice (Schädel et al., 2023). Using treadmills and other experimental equipment can force mice to exercise and achieve greater exercise benefits, but this can impose stress on the mice and even lead to mortality (Narath et al., 2001). Additionally, aging causes mice to become frailer, and obesity exacerbates this negative effect, further increasing their mortality rate (Zhang et al., 2015). Therefore, we chose a low-intensity CR combined with or without voluntary wheel running intervention for the mice to ensure the survival rate of the mice and the successful completion of the experiment. Furthermore, aging (Rattan & Derventzi, 1991) and obesity (de Wilde et al., 2009) lower the body's metabolic rate and responsiveness to external stimuli. The combined effects of these factors are the primary reasons for the lack of significant intervention results.

4.5 DR+Ex Regulated Ferroptosis Expression in Red Muscle

Although no significant regulatory effects of DR and DR+Ex on ferroptosis signals (4-HNE and MDA) in the wholly skeletal muscles of obese mice were found, expression did reduced. Therefore, we used WB analysis to examine the regulatory mechanisms of DR and DR+Ex on ferroptosis signals in different muscle types. The results showed that after DR+Ex, the expression of GPX4 in red muscle significantly increased in obese mice, whereas it did not in white muscle. This may be related to the oxidative stress, metabolic demands, and specific gene regulatory mechanisms of different skeletal muscle types.

Firstly, red muscle primarily relies on aerobic metabolism and is rich in mitochondria, adapting to prolonged low-intensity exercise. Studies have shown that antioxidant mechanisms in red muscle are more prominent, potentially leading to the easier expression of GPX4 in response to oxidative stress in this environment (Rinnankoski-Tuikka et al., 2012). Secondly, DR and Ex lead to increased aerobic metabolism activity in skeletal muscle, requiring more antioxidant protection to prevent lipid peroxidation damage (Civitarese et al., 2007; Galassetti et al., 2006). As a key antioxidant enzyme, GPX4 is upregulated in this context, while white muscle, which primarily relies on glycolysis for energy, has lower oxidative stress, and its GPX4 expression maybe does not significantly increase. Lastly, DR and Ex can regulate gene expression through specific signaling pathways such as AMPK and PGC-1α. These pathways are more active in red muscle (Gouspillou et al., 2014; Jørgensen et al., 2007; Pengam et al., 2020) and are related to the

expression of antioxidant enzymes. In summary, the increased expression of GPX4 in red muscle may be due to its high sensitivity to oxidative stress, higher metabolic demands, and specific gene regulation induced by endurance exercise. In contrast, white muscle, with its different metabolic characteristics, did not show the same changes in GPX4 expression.

We found that after DR+Ex in obese mice, the expression of AMPK decreased in white muscle but not in red muscle. This may be related to the metabolic differences between muscle fiber types, exercise-induced specific regulation, and the different impacts of diet and exercise on metabolic regulation. Red muscle primarily relies on aerobic metabolism, is rich in mitochondria, and is adapted to prolonged low-intensity exercise, maintaining high AMPK activity to meet its metabolic demands and antioxidant capacity. Under conditions of exercise and dietary restriction, AMPK expression remains stable in red muscle. In contrast, white muscle primarily relies on glycolysis for energy, has lower oxidative stress at resting stat, and therefore requires less AMPK, after intervention leading to a possible decrease in its expression (Jørgensen et al., 2007).

After DR and DR+Ex in obese mice, the expression of 4-HNE decreased in red muscle but not in white muscle. This difference is related to the metabolic differences between skeletal muscle types, specific gene regulation, and the specific effects of diet and exercise on red muscle. Red muscle primarily relies on aerobic metabolism, is rich in mitochondria, and is adapted to prolonged low-intensity exercise. Consequently, its metabolic activity and oxidative stress are higher, necessitating stronger antioxidant protection mechanisms. Studies have shown that red muscle significantly increases antioxidant enzyme activity under DR and Ex, reducing the production of oxidative stress markers such as 4-HNE (Jørgensen et al., 2007). Moreover, exercise regulates gene expression through specific signaling pathways which are more active in red muscle. This promotes the expression and activity of antioxidant enzymes, further reducing levels of oxidative stress markers (Sriwijitkamol et al., 2006).

We found that as an upstream signal and regulatory molecule of 4-HEN, the expression of GPX4 in red muscle significantly increased after intervention. Therefore, we suggest that DR and DR+Ex can regulate ferroptosis by altering the expression of GPX4 in red muscle, which in turn modulates the downstream expression of 4-HEN. However, AMPK, also an upstream regulatory molecule of 4-HEN, showed inconsistent expression changes with 4-HNE in white muscle. After a high-fat diet, the regulatory effect of AMPK on 4-HNE in white muscle was impaired, likely due to metabolic disturbances caused by obesity. This warrants further investigation in future studies.

5. Conclusion

Obesity induced by a high-fat diet leads to ferroptosis in the skeletal muscle of mice. The mechanism is muscle type-specific, with NCOA4 expression upregulated in red muscle and GPX4 expression upregulated in white muscle, ultimately triggering ferroptosis. Additionally, DR and DR+Ex can partially mitigate ferroptosis in the skeletal muscle of obese mice induced by a high-fat diet. This mechanism is achieved by regulating the expression of GPX4 in red muscle. Overall, we have identified muscle type-specific regulatory mechanisms of ferroptosis, providing molecular biology-related scientific data for the prevention and treatment of related diseases in the future.

6. limitation

The study focuses on the gastrocnemius muscle, which may not fully represent the effects of dietary restriction and exercise on other muscle groups, as different muscles may respond differently to these interventions. Additionally, the duration of dietary restriction and exercise intervention was limited to eight weeks. Longer-term studies are necessary to understand the chronic effects and sustainability of these interventions on ferroptosis and overall muscle health. Furthermore, incorporating advanced experimental tools, such as single-cell sequencing, could provide a more detailed and microscopic analysis of the results.

7. WB representative picture

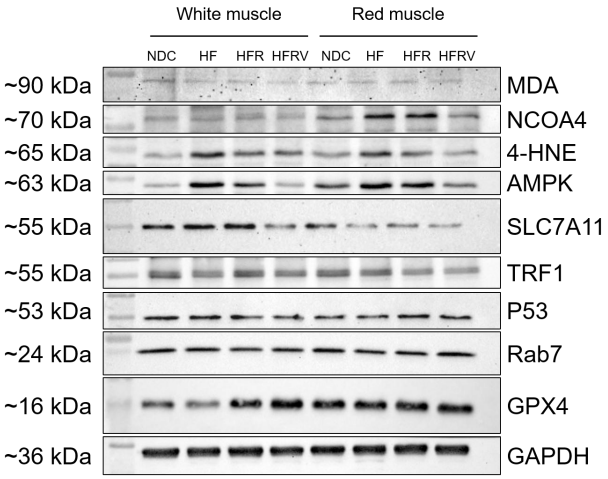

8. Ethical approval and consent to participate

All the procedures followed in this experiment were approved by the Institutional Animal Care and Use Committee (IACUC) of Hanyang University (HYU 2021-0066A).

9. Consent for publication

Not applicable.

10. Availability of data and materials

The data used to support the findings of this study are presented here. Any further data requirements are available from the corresponding author upon request.

11. Competing interests

No conflicts of interest, financial or otherwise, have been declared by the author(s).

12. Funding

This research was supported by the National Research Foundation of Korea (NRF-2020R1F1A1061726).

13. Author's contributions

F.J.J. and J.H.K. conceived and designed the study. F.J.J., Y.J.P. and H.s.L. performed the

experiments. F.J.J. and H.s.L. analyzed the data and prepared the figures. F.J.J. and J.H.K. interpreted the results, drafted, edited, and revised the manuscript. J.H.K. acquired funding. All authors approved the final version of the manuscript.

14. Acknowledgments

We thank Jian Guo (Hanyang University, Korea) for his generous help in dissecting the mice.
We are grateful to Prof. Dr. Gwang-woong Go (Hanyang University, Korea) for generously providing the DEXA machine for body composition analysis of the mice.
We thank the support of Skill Learning from Kaixin Doctor and MASCU (Medical Association with Science, Creativity, and Unity), Inc, Shenzhen, China (mascu_forever@163.com).

15. Reference

Ahmed, S., Maher, F., & Naji, N. (2016). Effect of leptin and oxidative stress in the blood of obese individuals. *Biochem Anal Biochem*, *5*(288), 2161-1009.

Armani, A., Cinti, F., Marzolla, V., Morgan, J., Cranston, G. A., Antelmi, A., Carpinelli, G., Canese, R., Pagotto, U., & Quarta, C. (2014). Mineralocorticoid receptor antagonism induces browning of white adipose tissue through impairment of autophagy and prevents adipocyte dysfunction in high-fat-diet-fed mice. *The FASEB Journal*, *28*(8), 3745-3757.

Ayala, A., Muñoz, M. F., & Argüelles, S. (2014). Lipid peroxidation: production, metabolism, and signaling mechanisms of malondialdehyde and 4-hydroxy-2-nonenal. *Oxidative Medicine and Cellular Longevity*, *2014*.

Bevilacqua, L., Ramsey, J. J., Hagopian, K., Weindruch, R., & Harper, M.-E. (2005). Long-term caloric restriction increases UCP3 content but decreases proton leak and reactive oxygen species production in rat skeletal muscle mitochondria. *American Journal of Physiology-Endocrinology and Metabolism*, *289*(3), E429-E438.

Blüher, M. (2019). Obesity: global epidemiology and pathogenesis. *Nature Reviews Endocrinology*, *15*(5), 288-298.

Buettner, R., Schölmerich, J., & Bollheimer, L. C. (2007). High-fat diets: modeling the metabolic disorders of human obesity in rodents. *Obesity*, *15*(4), 798-808.

Chen, D., Wang, Y., & Chin, E. R. (2015). Activation of the endoplasmic reticulum stress response in skeletal muscle of G93A*SOD1 amyotrophic lateral sclerosis mice. *Front Cell Neurosci*, *9*, 170. https://doi.org/10.3389/fncel.2015.00170

Chen, J., Zhu, T., Yu, D., Yan, B., Zhang, Y., Jin, J., Yang, Z., Zhang, B., Hao, X., & Chen, Z. (2023). Moderate intensity of treadmill exercise rescues TBI-induced ferroptosis, neurodegeneration, and cognitive impairments via suppressing STING pathway. *Molecular Neurobiology*, *60*(9), 4872-4896.

Chen, W., Wilson, J. L., Khaksari, M., Cowley, M. A., & Enriori, P. J. (2012). Abdominal fat analyzed by DEXA scan reflects visceral body fat and improves the phenotype description and the assessment of metabolic risk in mice. *Am J Physiol Endocrinol Metab*, *303*(5), E635-643. https://doi.org/10.1152/ajpendo.00078.2012

Chen, X., Comish, P. B., Tang, D., & Kang, R. (2021). Characteristics and Biomarkers of Ferroptosis. *Front Cell Dev Biol*, *9*, 637162. https://doi.org/10.3389/fcell.2021.637162

Chooi, Y. C., Ding, C., & Magkos, F. (2019). The epidemiology of obesity. *Metabolism*, *92*, 6-10. https://doi.org/10.1016/j.metabol.2018.09.005

609 Civitarese, A. E., Carling, S., Heilbronn, L. K., Hulver, M. H., Ukropcova, B., Deutsch, W. A., Smith, S. R.,
610 & Ravussin, E. (2007). Calorie restriction increases muscle mitochondrial biogenesis in
611 healthy humans. *PLoS medicine*, *4*(3), e76.
612 Collins, K. H., Herzog, W., MacDonald, G. Z., Reimer, R. A., Rios, J. L., Smith, I. C., Zernicke, R. F., & Hart,
613 D. A. (2018). Obesity, metabolic syndrome, and musculoskeletal disease: common
614 inflammatory pathways suggest a central role for loss of muscle integrity. *Frontiers in*
615 *physiology*, *9*, 112.
616 de Wilde, J., Smit, E., Mohren, R., Boekschoten, M. V., de Groot, P., van den Berg, S. A., Bijland, S.,
617 Voshol, P. J., van Dijk, K. W., de Wit, N. W., Bunschoten, A., Schaart, G., Hulshof, M. F., &
618 Mariman, E. C. (2009). An 8-week high-fat diet induces obesity and insulin resistance with
619 small changes in the muscle transcriptome of C57BL/6J mice. *J Nutrigenet Nutrigenomics*,
620 *2*(6), 280-291. https://doi.org/10.1159/000308466
621 Del Rio, D., Stewart, A. J., & Pellegrini, N. (2005). A review of recent studies on malondialdehyde as
622 toxic molecule and biological marker of oxidative stress. *Nutr Metab Cardiovasc Dis*, *15*(4),
623 316-328. https://doi.org/10.1016/j.numecd.2005.05.003
624 Ding, H., Chen, S., Pan, X., Dai, X., Pan, G., Li, Z., Mai, X., Tian, Y., Zhang, S., Liu, B., Cao, G., Yao, Z., Yao,
625 X., Gao, L., Yang, L., Chen, X., Sun, J., Chen, H., Han, M., . . . Xie, L. (2021). Transferrin receptor
626 1 ablation in satellite cells impedes skeletal muscle regeneration through activation of
627 ferroptosis. *J Cachexia Sarcopenia Muscle*, *12*(3), 746-768.
628 https://doi.org/10.1002/jcsm.12700
629 Dixon, S. J., Lemberg, K. M., Lamprecht, M. R., Skouta, R., Zaitsev, E. M., Gleason, C. E., Patel, D. N.,
630 Bauer, A. J., Cantley, A. M., & Yang, W. S. (2012). Ferroptosis: an iron-dependent form of
631 nonapoptotic cell death. *cell*, *149*(5), 1060-1072.
632 Dowdle, W. E., Nyfeler, B., Nagel, J., Elling, R. A., Liu, S., Triantafellow, E., Menon, S., Wang, Z., Honda,
633 A., Pardee, G., Cantwell, J., Luu, C., Cornella-Taracido, I., Harrington, E., Fekkes, P., Lei, H.,
634 Fang, Q., Digan, M. E., Burdick, D., . . . Murphy, L. O. (2014). Selective VPS34 inhibitor blocks
635 autophagy and uncovers a role for NCOA4 in ferritin degradation and iron homeostasis in vivo.
636 *Nature cell biology*, *16*(11), 1069-1079. https://doi.org/10.1038/ncb3053
637 Endale, H. T., Tesfaye, W., & Mengstie, T. A. (2023). ROS induced lipid peroxidation and their role in
638 ferroptosis. *Frontiers in cell and Developmental Biology*, *11*.
639 Esterbauer, H., Schaur, R. J., & Zollner, H. (1991). Chemistry and biochemistry of 4-hydroxynonenal,
640 malonaldehyde and related aldehydes. *Free Radic Biol Med*, *11*(1), 81-128.
641 https://doi.org/10.1016/0891-5849(91)90192-6
642 Fang, D., Wang, Y., Zhang, Z., Yang, D., Gu, D., He, B., Zhang, X., He, D., Wang, H., & Jose, P. A. (2021).
643 Calorie restriction protects against contrast-induced nephropathy via SIRT1/GPX4 activation.
644 *Oxidative Medicine and Cellular Longevity*, *2021*(1), 2999296.
645 Fang, X., Cai, Z., Wang, H., Han, D., Cheng, Q., Zhang, P., Gao, F., Yu, Y., Song, Z., & Wu, Q. (2020). Loss
646 of cardiac ferritin H facilitates cardiomyopathy via Slc7a11-mediated ferroptosis. *Circulation*
647 *research*, *127*(4), 486-501.
648 Franco-Romero, A., Sandri, M., & Schiaffino, S. (2024). Autophagy in Skeletal Muscle. *Cold Spring*
649 *Harbor Perspectives in Biology*, a041565.
650 Friedmann Angeli, J. P., Schneider, M., Proneth, B., Tyurina, Y. Y., Tyurin, V. A., Hammond, V. J., Herbach,
651 N., Aichler, M., Walch, A., & Eggenhofer, E. (2014). Inactivation of the ferroptosis regulator
652 Gpx4 triggers acute renal failure in mice. *Nature cell biology*, *16*(12), 1180-1191.

653 Galassetti, P. R., Nemet, D., Pescatello, A., Rose-Gottron, C., Larson, J., & Cooper, D. M. (2006). Exercise,
654 caloric restriction, and systemic oxidative stress. *Journal of investigative medicine*, *54*(2),
655 67-75.
656 Ganz, T. (2012). Macrophages and systemic iron homeostasis. *Journal of innate immunity*, *4*(5-6),
657 446-453.
658 Gouspillou, G., Sgarioto, N., Norris, B., Barbat-Artigas, S., Aubertin-Leheudre, M., Morais, J. A., Burelle,
659 Y., Taivassalo, T., & Hepple, R. T. (2014). The relationship between muscle fiber type-specific
660 PGC-1α content and mitochondrial content varies between rodent models and humans. *PloS*
661 *one*, *9*(8), e103044. https://doi.org/10.1371/journal.pone.0103044
662 Graham, L. C., Grabowska, W. A., Chun, Y., Risacher, S. L., Philip, V. M., Saykin, A. J., Rizzo, S. J. S.,
663 Howell, G. R., & Initiative, A. s. D. N. (2019). Exercise prevents obesity-induced cognitive
664 decline and white matter damage in mice. *Neurobiology of aging*, *80*, 154-172.
665 Guerrero-Hue, M., García-Caballero, C., Palomino-Antolín, A., Rubio-Navarro, A., Vázquez-Carballo, C.,
666 Herencia, C., Martín-Sanchez, D., Farré-Alins, V., Egea, J., Cannata, P., Praga, M., Ortiz, A.,
667 Egido, J., Sanz, A. B., & Moreno, J. A. (2019). Curcumin reduces renal damage associated with
668 rhabdomyolysis by decreasing ferroptosis-mediated cell death. *Faseb j*, *33*(8), 8961-8975.
669 https://doi.org/10.1096/fj.201900077R
670 Han, C., Lee, S., Lim, S., Kong, H., Kim, S., Lee, S., & Chang, J. (2006). Studies on production of high fat
671 diet induced obesity C57BL/6NCrjBgi mice. *Laboratory Animal Research*, *22*(3), 221-226.
672 Hariri, N., & Thibault, L. (2010). High-fat diet-induced obesity in animal models. *Nutrition research*
673 *reviews*, *23*(2), 270-299.
674 Hart, C. R., Layec, G., Trinity, J. D., Kwon, O. S., Zhao, J., Reese, V. R., Gifford, J. R., & Richardson, R. S.
675 (2018). Increased skeletal muscle mitochondrial free radical production in peripheral arterial
676 disease despite preserved mitochondrial respiratory capacity. *Exp Physiol*, *103*(6), 838-850.
677 https://doi.org/10.1113/ep086905
678 He, F., Huang, X., Wei, G., Lin, X., Zhang, W., Zhuang, W., He, W., Zhan, T., Hu, H., & Yang, H. (2022).
679 Regulation of ACSL4-catalyzed lipid peroxidation process resists cisplatin ototoxicity.
680 *Oxidative Medicine and Cellular Longevity*, *2022*.
681 He, L. P., Zhou, Z. X., & Li, C. P. (2023). Narrative review of ferroptosis in obesity. *Journal of Cellular and*
682 *Molecular Medicine*, *27*(7), 920-926.
683 Hotamisligil, G. S. (2006). Inflammation and metabolic disorders. *Nature*, *444*(7121), 860-867.
684 Huang, Y., Wu, B., Shen, D., Chen, J., Yu, Z., & Chen, C. (2021). Ferroptosis in a sarcopenia model of
685 senescence accelerated mouse prone 8 (SAMP8). *Int J Biol Sci*, *17*(1), 151-162.
686 https://doi.org/10.7150/ijbs.53126
687 Ji, F., Park, J. H., Rheem, H., & Kim, J.-H. (2024). Overlapping and Distinct Physical and Biological
688 Phenotypes Related to Pure Frailty and Frail Obesity. *Bioscience Reports*, BSR20240784.
689 Jørgensen, S. B., Treebak, J. T., Viollet, B., Schjerling, P., Vaulont, S., Wojtaszewski, J. F., & Richter, E. A.
690 (2007). Role of AMPKα2 in basal, training-, and AICAR-induced GLUT4, hexokinase II, and
691 mitochondrial protein expression in mouse muscle. *American Journal of*
692 *Physiology-Endocrinology and Metabolism*, *292*(1), E331-E339.
693 Justice, J. N., Cesari, M., Seals, D. R., Shively, C. A., & Carter, C. S. (2016). Comparative Approaches to
694 Understanding the Relation Between Aging and Physical Function. *J Gerontol A Biol Sci Med*
695 *Sci*, *71*(10), 1243-1253. https://doi.org/10.1093/gerona/glv035

696 Kalinkovich, A., & Livshits, G. (2017). Sarcopenic obesity or obese sarcopenia: a cross talk between
697 age-associated adipose tissue and skeletal muscle inflammation as a main mechanism of the
698 pathogenesis. *Ageing research reviews*, *35*, 200-221.
699 Kang, R., Zeng, L., Xie, Y., Yan, Z., Zhou, B., Cao, L., Klionsky, D. J., Tracey, K. J., Li, J., & Wang, H. (2016).
700 A novel PINK1-and PARK2-dependent protective neuroimmune pathway in lethal sepsis.
701 *Autophagy*, *12*(12), 2374-2385.
702 Katunga, L. A., Gudimella, P., Efird, J. T., Abernathy, S., Mattox, T. A., Beatty, C., Darden, T. M., Thayne, K.
703 A., Alwair, H., Kypson, A. P., Virag, J. A., & Anderson, E. J. (2015). Obesity in a model of gpx4
704 haploinsufficiency uncovers a causal role for lipid-derived aldehydes in human metabolic
705 disease and cardiomyopathy. *Mol Metab*, *4*(6), 493-506.
706 https://doi.org/10.1016/j.molmet.2015.04.001
707 Khachatoorian, Y., & Samara, A. (2018). Differential effects of dietary restriction combined with
708 exercise vs dietary restriction alone on visceral and subcutaneous adipose tissues: A
709 systematic review. *Obesity Medicine*, *9*, 7-17.
710 Kim, J. D., McCarter, R. J., & Yu, B. P. (1996). Influence of age, exercise, and dietary restriction on
711 oxidative stress in rats. *Aging (Milano)*, *8*(2), 123-129. https://doi.org/10.1007/bf03339566
712 Koza, R. A., Nikonova, L., Hogan, J., Rim, J. S., Mendoza, T., Faulk, C., Skaf, J., & Kozak, L. P. (2006).
713 Changes in gene expression foreshadow diet-induced obesity in genetically identical mice.
714 *PLoS Genet*, *2*(5), e81. https://doi.org/10.1371/journal.pgen.0020081
715 Kvedaras, M., Minderis, P., Krusnauskas, R., & Ratkevicius, A. (2020). Effects of ten-week 30% caloric
716 restriction on metabolic health and skeletal muscles of adult and old C57BL/6J mice.
717 *Mechanisms of Ageing and Development*, *190*, 111320.
718 Li, C., Feng, F., Xiong, X., Li, R., & Chen, N. (2017). Exercise coupled with dietary restriction reduces
719 oxidative stress in male adolescents with obesity. *Journal of sports sciences*, *35*(7), 663-668.
720 Lin, P.-Y., Romsos, D. R., & Leveille, G. A. (1977). Food intake, body weight gain, and body composition
721 of the young obese (ob/ob) mouse. *The Journal of Nutrition*, *107*(9), 1715-1723.
722 Liu, T., Cui, Y., Dong, S., Kong, X., Xu, X., Wang, Y., Wan, Q., & Wang, Q. (2022). Treadmill training
723 reduces cerebral ischemia-reperfusion injury by inhibiting ferroptosis through activation of
724 SLC7A11/GPX4. *Oxidative Medicine and Cellular Longevity*, *2022*.
725 Ma, X., Pham, V. T., Mori, H., MacDougald, O. A., Shah, Y. M., & Bodary, P. F. (2017). Iron elevation and
726 adipose tissue remodeling in the epididymal depot of a mouse model of polygenic obesity.
727 *PloS one*, *12*(6), e0179889.
728 Magaki, S., Hojat, S. A., Wei, B., So, A., & Yong, W. H. (2019). An Introduction to the Performance of
729 Immunohistochemistry. *Methods Mol Biol*, *1897*, 289-298.
730 https://doi.org/10.1007/978-1-4939-8935-5_25
731 Mancias, J. D., Wang, X., Gygi, S. P., Harper, J. W., & Kimmelman, A. C. (2014). Quantitative proteomics
732 identifies NCOA4 as the cargo receptor mediating ferritinophagy. *Nature*, *509*(7498),
733 105-109.
734 Mandarim-de-Lacerda, C. A., Del Sol, M., Vazquez, B., & Aguila, M. B. (2021). Mice as an animal model
735 for the study of adipose tissue and obesity. *Int J Morphol*, *39*(6), 1521-1528.
736 Mizushima, N. (2007). Autophagy: process and function. *Genes & development*, *21*(22), 2861-2873.
737 Morris, R. T., Laye, M. J., Lees, S. J., Rector, R. S., Thyfault, J. P., & Booth, F. W. (2008). Exercise-induced
738 attenuation of obesity, hyperinsulinemia, and skeletal muscle lipid peroxidation in the OLETF
739 rat. *J Appl Physiol (1985)*, *104*(3), 708-715. https://doi.org/10.1152/japplphysiol.01034.2007

740 Murdolo, G., Bartolini, D., Tortoioli, C., Vermigli, C., Piroddi, M., & Galli, F. (2023). Accumulation of
741 4-Hydroxynonenal Characterizes Diabetic Fat and Modulates Adipogenic Differentiation of
742 Adipose Precursor Cells. *International Journal of Molecular Sciences*, *24*(23), 16645.
743 Narath, E., Skalicky, M., & Viidik, A. (2001). Voluntary and forced exercise influence the survival and
744 body composition of ageing male rats differently. *Experimental gerontology*, *36*(10),
745 1699-1711.
746 Orr, J. S., Kennedy, A., Anderson-Baucum, E. K., Webb, C. D., Fordahl, S. C., Erikson, K. M., Zhang, Y.,
747 Etzerodt, A., Moestrup, S. K., & Hasty, A. H. (2014). Obesity alters adipose tissue macrophage
748 iron content and tissue iron distribution. *Diabetes*, *63*(2), 421-432.
749 Ostler, J. E., Maurya, S. K., Dials, J., Roof, S. R., Devor, S. T., Ziolo, M. T., & Periasamy, M. (2014). Effects
750 of insulin resistance on skeletal muscle growth and exercise capacity in type 2 diabetic mouse
751 models. *American Journal of Physiology-Endocrinology and Metabolism*, *306*(6), E592-E605.
752 Park, M. W., Cha, H. W., Kim, J., Kim, J. H., Yang, H., Yoon, S., Boonpraman, N., Yi, S. S., Yoo, I. D., &
753 Moon, J.-S. (2021). NOX4 promotes ferroptosis of astrocytes by oxidative stress-induced lipid
754 peroxidation via the impairment of mitochondrial metabolism in Alzheimer's diseases. *Redox*
755 *biology*, *41*, 101947.
756 Pengam, M., Moisan, C., Simon, B., Guernec, A., Inizan, M., & Amérand, A. (2020). Training protocols
757 differently affect AMPK-PGC-1α signaling pathway and redox state in trout muscle. *Comp*
758 *Biochem Physiol A Mol Integr Physiol*, *243*, 110673.
759 https://doi.org/10.1016/j.cbpa.2020.110673
760 Ramana, K. V., Srivastava, S., & Singhal, S. S. (2014). Lipid peroxidation products in human health and
761 disease 2014. *Oxid Med Cell Longev*, *2014*, 162414. https://doi.org/10.1155/2014/162414
762 Rattan, S. I., & Derventzi, A. (1991). Altered cellular responsiveness during ageing. *Bioessays*, *13*(11),
763 601-606.
764 Rinnankoski-Tuikka, R., Silvennoinen, M., Torvinen, S., Hulmi, J. J., Lehti, M., Kivelä, R., Reunanen, H., &
765 Kainulainen, H. (2012). Effects of high-fat diet and physical activity on pyruvate
766 dehydrogenase kinase-4 in mouse skeletal muscle. *Nutrition & metabolism*, *9*, 1-13.
767 Rogers, P., & Webb, G. P. (1980). Estimation of body fat in normal and obese mice. *British Journal of*
768 *Nutrition*, *43*(1), 83-86.
769 Ruegsegger, G. N., & Booth, F. W. (2018). Health benefits of exercise. *Cold Spring Harbor perspectives*
770 *in medicine*, *8*(7), a029694.
771 Savira, M., Rusdiana, S. S. W., & Syahputra, M. (2020). Comparison Malondialdehyde (MDA) Level
772 between Obesity Non Metabolic Syndrome and Obesity with Metabolic Syndrome Patients.
773 *Age*, *53*(11.3), 44.55-10.48.
774 Schädel, P., Wichmann-Costaganna, M., Czapka, A., Gebert, N., Ori, A., & Werz, O. (2023). Short-Term
775 Caloric Restriction and Subsequent Re-Feeding Compromise Liver Health and Associated Lipid
776 Mediator Signaling in Aged Mice. *Nutrients*, *15*(16), 3660.
777 Shi, Y., Zhong, L., Liu, Y., Xu, S., Dai, J., Zhang, Y., & Hu, Y. (2024). Dietary sanguinarine supplementation
778 recovers the decrease in muscle quality and nutrient composition induced by high-fat diets of
779 grass carp (Ctenopharyngodon idella). *Animal Nutrition*, *17*, 208-219.
780 https://doi.org/https://doi.org/10.1016/j.aninu.2024.04.001
781 Shortreed, K. E., Krause, M. P., Huang, J. H., Dhanani, D., Moradi, J., Ceddia, R. B., & Hawke, T. J. (2009).
782 Muscle-specific adaptations, impaired oxidative capacity and maintenance of contractile
783 function characterize diet-induced obese mouse skeletal muscle. *PloS one*, *4*(10), e7293.

Sriwijitkamol, A., Ivy, J. L., Christ-Roberts, C., DeFronzo, R. A., Mandarino, L. J., & Musi, N. (2006). LKB1-AMPK signaling in muscle from obese insulin-resistant Zucker rats and effects of training. *American Journal of Physiology-Endocrinology and Metabolism*, *290*(5), E925-E932.

Stockwell, B. R. (2022). Ferroptosis turns 10: Emerging mechanisms, physiological functions, and therapeutic applications. *cell*, *185*(14), 2401-2421.

Stockwell, B. R., Angeli, J. P. F., Bayir, H., Bush, A. I., Conrad, M., Dixon, S. J., Fulda, S., Gascón, S., Hatzios, S. K., & Kagan, V. E. (2017). Ferroptosis: a regulated cell death nexus linking metabolism, redox biology, and disease. *cell*, *171*(2), 273-285.

Stockwell, B. R., & Jiang, X. (2019). A physiological function for ferroptosis in tumor suppression by the immune system. *Cell Metabolism*, *30*(1), 14-15.

Stringer, C., Wang, T., Michaelos, M., & Pachitariu, M. (2021). Cellpose: a generalist algorithm for cellular segmentation. *Nature Methods*, *18*(1), 100-106. https://doi.org/10.1038/s41592-020-01018-x

Suga, T., Kinugawa, S., Takada, S., Kadoguchi, T., Fukushima, A., Homma, T., Masaki, Y., Furihata, T., Takahashi, M., & Sobirin, M. A. (2014). Combination of exercise training and diet restriction normalizes limited exercise capacity and impaired skeletal muscle function in diet-induced diabetic mice. *Endocrinology*, *155*(1), 68-80.

Tang, D., Chen, X., Kang, R., & Kroemer, G. (2021). Ferroptosis: molecular mechanisms and health implications. *Cell Research*, *31*(2), 107-125. https://doi.org/10.1038/s41422-020-00441-1

Vellers, H. L., Letsinger, A. C., Walker, N. R., Granados, J. Z., & Lightfoot, J. T. (2017). High Fat High Sugar Diet Reduces Voluntary Wheel Running in Mice Independent of Sex Hormone Involvement. *Front Physiol*, *8*, 628. https://doi.org/10.3389/fphys.2017.00628

Walsh, M. E., Shi, Y., & Van Remmen, H. (2014). The effects of dietary restriction on oxidative stress in rodents. *Free Radical Biology and Medicine*, *66*, 88-99.

Wang, H., An, P., Xie, E., Wu, Q., Fang, X., Gao, H., Zhang, Z., Li, Y., Wang, X., & Zhang, J. (2017). Characterization of ferroptosis in murine models of hemochromatosis. *Hepatology*, *66*(2), 449-465.

Weisberg, S. P., McCann, D., Desai, M., Rosenbaum, M., Leibel, R. L., & Ferrante, A. W. (2003). Obesity is associated with macrophage accumulation in adipose tissue. *The Journal of clinical investigation*, *112*(12), 1796-1808.

Wenzel, S. E., Tyurina, Y. Y., Zhao, J., Croix, C. M. S., Dar, H. H., Mao, G., Tyurin, V. A., Anthonymuthu, T. S., Kapralov, A. A., & Amoscato, A. A. (2017). PEBP1 wardens ferroptosis by enabling lipoxygenase generation of lipid death signals. *cell*, *171*(3), 628-641. e626.

Xiang, Y.-Y., Baek, K.-W., Won, J.-H., Park, Y., Kim, J.-S., Xiang, Y.-Y., Baek, K.-W., Won, J.-H., Park, Y., & Kim, J.-S. (2023). Effects of Lifelong Aerobic Exercise on Ferroptosis-Related Gene Expressions in Kidney of Aged Mice. *Exercise Science*, *32*(4), 410-418.

Yang, W. S., SriRamaratnam, R., Welsch, M. E., Shimada, K., Skouta, R., Viswanathan, V. S., Cheah, J. H., Clemons, P. A., Shamji, A. F., & Clish, C. B. (2014). Regulation of ferroptotic cancer cell death by GPX4. *cell*, *156*(1), 317-331.

Yang, Y., Smith, D. L., Jr., Keating, K. D., Allison, D. B., & Nagy, T. R. (2014). Variations in body weight, food intake and body composition after long-term high-fat diet feeding in C57BL/6J mice. *Obesity (Silver Spring)*, *22*(10), 2147-2155. https://doi.org/10.1002/oby.20811

826 Yang, Y., Smith Jr, D. L., Keating, K. D., Allison, D. B., & Nagy, T. R. (2014). Variations in body weight,
827 food intake and body composition after long-term high-fat diet feeding in C57BL/6J mice.
828 *Obesity*, *22*(10), 2147-2155.
829 Yeu, J., Ko, H. J., Kim, D., Ahn, Y., Kim, J., Lee, W., Jung, I., Suh, J., & Lee, S. J. (2019). Evaluation of
830 iNSiGHT VET DXA (Dual-Energy X-ray Absorptiometry) for assessing body composition in
831 obese rats fed with high fat diet: a follow-up study of diet induced obesity model for 8 weeks.
832 *Lab Anim Res*, *35*, 2. https://doi.org/10.1186/s42826-019-0004-2
833 Yu, Y., Jiang, L., Wang, H., Shen, Z., Cheng, Q., Zhang, P., Wang, J., Wu, Q., Fang, X., & Duan, L. (2020).
834 Hepatic transferrin plays a role in systemic iron homeostasis and liver ferroptosis. *Blood, The*
835 *Journal of the American Society of Hematology*, *136*(6), 726-739.
836 Zhang, X., Ma, Y., Lv, G., & Wang, H. (2023). Ferroptosis as a therapeutic target for
837 inflammation-related intestinal diseases. *Front Pharmacol*, *14*, 1095366.
838 https://doi.org/10.3389/fphar.2023.1095366
839 Zhang, Y., Fischer, K. E., Soto, V., Liu, Y., Sosnowska, D., Richardson, A., & Salmon, A. B. (2015).
840 Obesity-induced oxidative stress, accelerated functional decline with age and increased
841 mortality in mice. *Archives of biochemistry and biophysics*, *576*, 39-48.
842 Zhao, X., Si, L., Bian, J., Pan, C., Guo, W., Qin, P., Zhu, W., Xia, Y., Zhang, Q., & Wei, K. (2022). Adipose
843 tissue macrophage-derived exosomes induce ferroptosis via glutathione synthesis inhibition
844 by targeting SLC7A11 in obesity-induced cardiac injury. *Free Radical Biology and Medicine*,
845 *182*, 232-245.
846 Zhuang, A., Yang, C., Liu, Y., Tan, Y., Bond, S. T., Walker, S., Sikora, T., Laskowski, A., Sharma, A., de Haan,
847 J. B., Meikle, P. J., Shimizu, T., Coughlan, M. T., Calkin, A. C., & Drew, B. G. (2021). SOD2 in
848 skeletal muscle: New insights from an inducible deletion model. *Redox Biol*, *47*, 102135.
849 https://doi.org/10.1016/j.redox.2021.102135